1

Visualization Paradigms

Chandrajit L. Bajaj
University of Texas, Austin

ABSTRACT

A wide variety of techniques have been developed for the visualization of scalar, vector and tensor field data. They range from volume visualization, to isocontouring, from vector field streamlines or scalar, vector and tensor topology, to function on surfaces . This multiplicity of approaches responds to the requirements emerging from an even wider range of application areas such as computational fluid dynamics, chemical transport, fracture mechanics, new material development, electromagnetic scattering/absorption, neuro-surgery, orthopedics, drug design. In this chapter I present a brief overview of the visualization paradigms currently used in several of the above application areas. A major objective is to provide a roadmap that encompasses the majority of the currently available methods to allow each potential user/developer to select the techniques suitable for his purpose.

1.1 Introduction

Typically, informative visualizations are based on the combined use of multiple techniques. For example figure 1.1 shows the combined use of isocontouring, volume rendering and slicing to highlight and compare the internal 3D structure of three different vorticity fields. For a detailed description of each of the approaches we make reference to subsequent chapters in this book and previously published technical papers and books [Bow95, Cle93, HU94, KK93, NHM97, REE+94, Wat92].

DATA VISUALIZATION TECHNIQUES, Edited by C. Bajaj

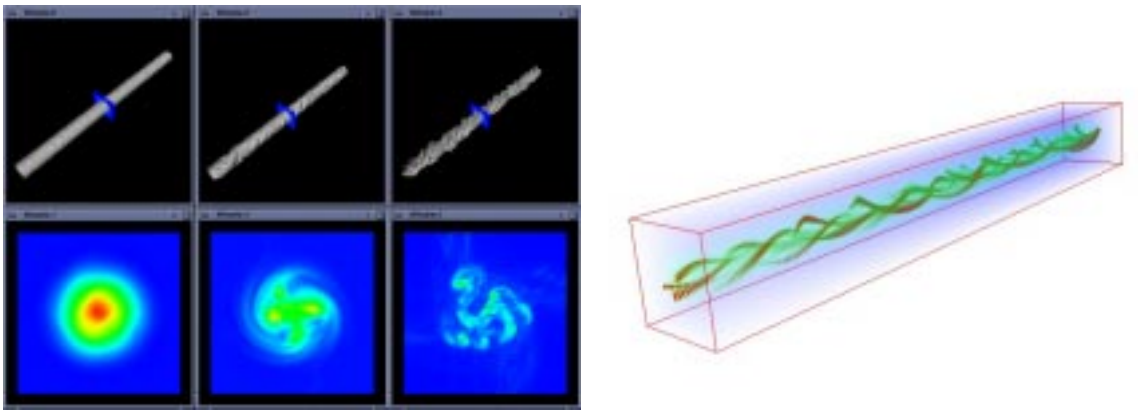

Figure 1.1 The combined display of isocontours, slicing and volume rendering used to highlight the 3D structure of vorticity fields.

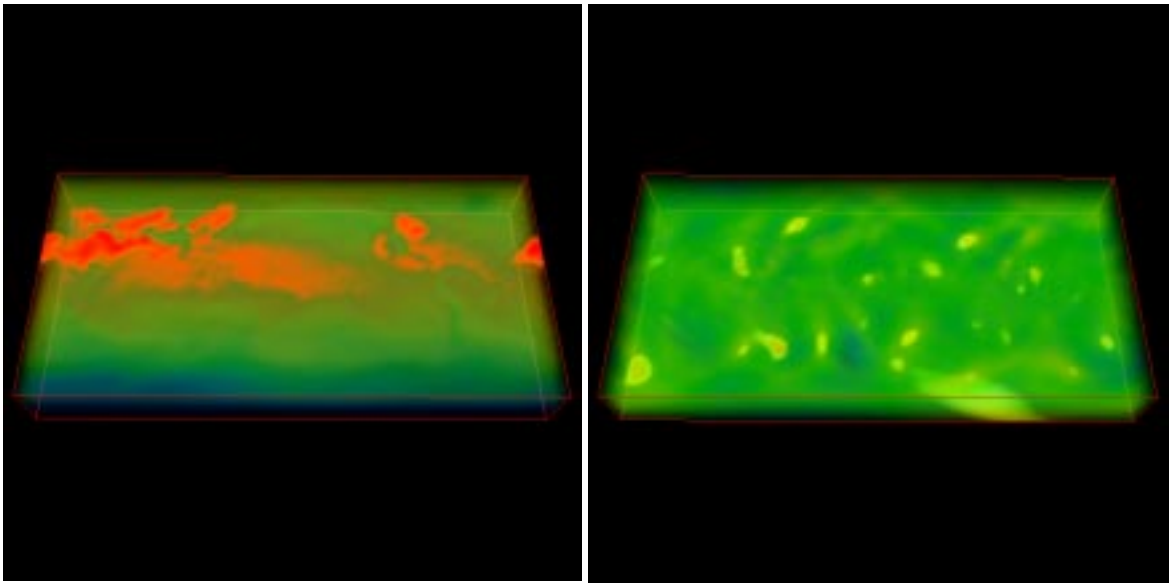

Figure 1.2 Two volume renderings showing snapshots of wind speed in a global climate model.

1.2 Volume Rendering

Volume rendering is a projection technique that produces image displays of three-dimensional volumetric data (see fig. 1.2). Its main characteristic is the production of view-dependent snapshots of volumetric data, rather than the extraction of geometric information such as isocontouring.

Chapter 2 surveys alternate volume rendering algorithms reported in the literature. Two main classes of approaches that have been developed differ mainly on the order

of projection of the volume cells. Secondary distinctions arise from the differences in color accumulation and composition techniques to produce the final image.

Forward projection techniques traverse the volume (object space approach) projecting and display each volumetric cell or voxel. This approach takes advantage of graphics hardware acceleration by selecting appropriate drawing primitives to approximate the voxel image.

Backward projection techniques traverse the image (image space approach) and cast through the data volume, one light ray per pixel, accumulating color intensities along the ray to determine the final pixel color.

Cell projection and splatting are both forward projection techniques. In cell projection, the cells of the data volume are traversed and their images computed by subdivision into a polygonal approximation. In splatting, the samples of the volume are traversed and their contribution to the final image is computed by convolution with a reconstruction kernel. Cell projection technique can be optimized by taking advantage of the spatial coherence of the volume cells both in the case of regular grids and in the case of unstructured meshes. Splatting has been shown to be a fast technique for hardware assisted scalar volume visualization, and was extended to vector fields (see details in Chapter 5) Additional splatting techniques are developed for texture based visualization of velocity fields in the vicinity of contour surfaces (see details in Chapter 6)

Backward projection methods are accelerated by exploiting the coherence between adjacent rays. This idea has been implemented in a number of approaches using: (i) adaptive sampling along the rays depending on the "importance" of different regions(ii) templating the paths of parallel rays through regular grids,(iii) bounding with simple polyhedra significant regions that give the main contribution to the output image, or (iv) maintaining the front of propagating rays through irregular grids. The high computational cost of volume rendering in the spatial domain can sometimes be replaced by an asymptotically faster computation in the frequency domain [Lev92, Mal93, TL93].

1.3 Isocontouring

Isocontouring is the extraction of constant valued curves and surfaces from 2d and 3d scalar fields. Interactive display and quantitative interrogation of isocontours helps in determining the overall structure of a scalar field (see fig. 1.3) and its evolution over time (see fig. 1.4).

Chapter 3 surveys the most commonly used isocontouring algorithms along with recent improvements that permit rapid evaluation of multiple isocontour queries, in an interactive environment. Traditional isocontouring techniques examine each cell of a mesh to test for intersection with the isocontour of interest. Accelerated isocontouring can be achieved by preprocessing the input scalar field both in its domain (the geometry of the input mesh) and in its range (the values of the sampled scalar field).

One the one hand, one takes advantage of the known adjacency information of mesh cells (domain space optimization). Given a single cell c on an isocontour component one can trace the entire isocontour component from c, by propagating from cell to cell

using inter-cell adjacency. This reduces the search for isocontour components from a search in the entire input mesh to a search in a much smaller subset called the *seed set*. A *seed set* is a subset of the mesh cells which has at least one cell on each connected component of each isocontour. From this typically very small seed set of mesh cells one searches for starting cells for each component of the desired isocontour and then applies contour propagation through cell adjacencies.

On the other hand, one independently optimizes the search for isocontours exploiting the simplicity of the range of the scalar field (range space optimization). The values of the field are scalars that in range space form an interval. Within each cell of the mesh (or of mesh cells of the seed set) the scalar field usually has a small continuous variation that can be represented in range space as a (small) subinterval. The isocontour computation is hence reduced in range space to the search for all the segments that intersect the currently selected isovalue w. This search can be optimally performed using well known interval tree or segment tree data structures.

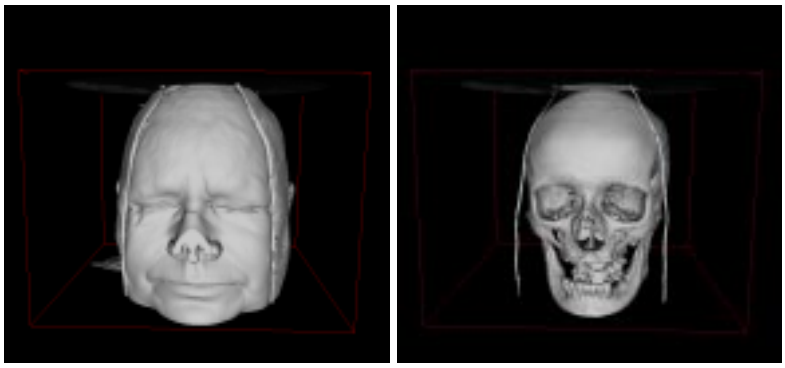

Figure 1.3 Skin and bone head models extracted as two different isocontours from the same volumetric MRI data of the Visible Human female.

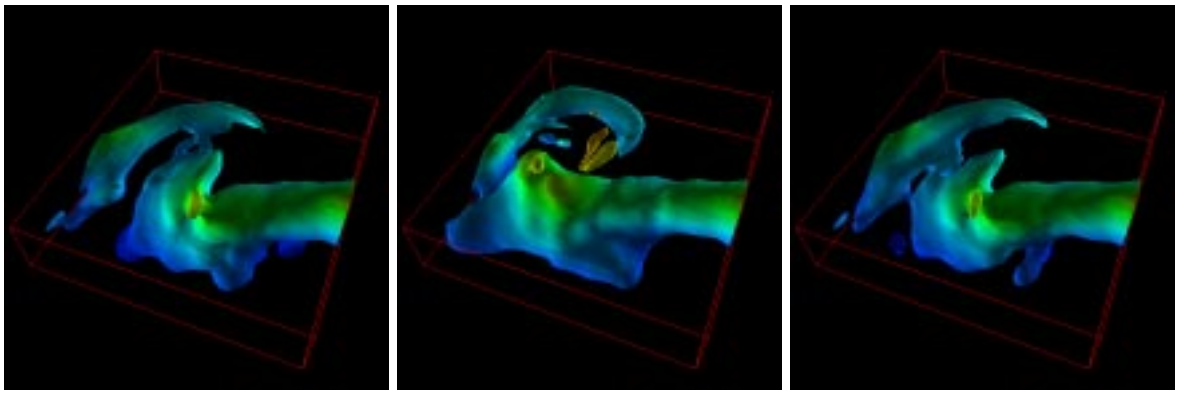

Figure 1.4 Three isocontours of wind speed that show the time evolution of air dynamics in a global climate model.

1.4 Flow Visualization

Visualization of vector fields is generally more complicated than visualizing scalar fields due to the increased amount of information inherent in vector data. Clearly vector data can be contracted to scalar quantities, for example by computation of vector magnitude, scalar product with a given vector, or magnitude of vorticity. In this case, scalar visualization techniques such as isosurfaces and volume rendering can be applied. Additional approaches to visualization of vector fields include iconography, particle tracking, and qualitative global flow visualization techniques. Chapter 5 reviews flow visualization techniques while Chapter 6 describes more in detail the approaches designed to take advantage of currently existing graphics hardware to increase performance. For additional detail, refer to the papers cited in these two chapters.

Particle tracking or advection techniques are based on following the trajectory of a theoretically massless particle in a flow. In its simplest form, the path traversed by a particle in a steady flow is called a *streamline*. If the flow is unsteady, or time-varying, the path followed by a particle over time is called a *path line*. A curve resulting from a number of particles emitted at regular or irregular intervals from a single source is called a *streak line*. Numerical techniques commonly used for evaluating the above equation include Euler and Runge-Kutta methods. In the case of incompressible flow, a single stream-function in 2D can be constructed such that the contours of the stream-function are streamlines of the vector field. In 3D, a pair of dual stream functions is required, and streamlines will occur as the intersections of isocontours of the two functions [KM92].

Particle tracking techniques may also be extended by grouping multiple particles together to form a *stream ribbon*, *stream surface*, *stream tube* or *flow volume*. Global techniques such as Line Integral Convolution present a qualitative view of the vector field which presents intuitively meaningful visualizations for the user. Flow "probes" may be placed at user-specified or computed locations to reveal local properties of the flow field such as direction, speed, divergence, vorticity, etc. Properties are mapped to a geometric representation called an *icon*. The complexity of the icon increases with the amount of information that it is designed to represent. Representing curl (vorticity), which is itself a vector field with additional physical meaning, can be achieved by a cylindrical icon with candystriping to indicate both the direction and magnitude of vorticity.

1.5 Quantification

In the quest for interrogative visualization [Baj88], in which the user can not only see the data, but navigate and query for increased understanding, the ability to quantify and perform volumetric measurements is vital. Another challenge to visualization is to give quantitative information concerning time dependent studies and time-varying structures (e.g. flow). In the study of paralysis, researchers are constructing models of spinal cords and regions of damaged cord from histological samples. Figure 1.5 (left) is an example of a histological slice of an injured rat spine. In Figure 1.5 (right), the damaged region has been reconstructed as a surface, and is visualized along with orthogonal slices of the 3D histological specimen. Traditionally, spinal damage has been

modelled as an expanding cylindrical region. The ability to more accurately define the region of damage and measure the surface area and volume of the region are promising tools in developing a greater understanding of cysts and how they develop.

Chapter 7 reviews tissue classification techniques using local reconstructions of band limited samplings, and Bayesian statistics. Such classification provides the means to accurately identify (for isocontouring and volume rendering), and quantify the relevant substructures of three dimensional images.

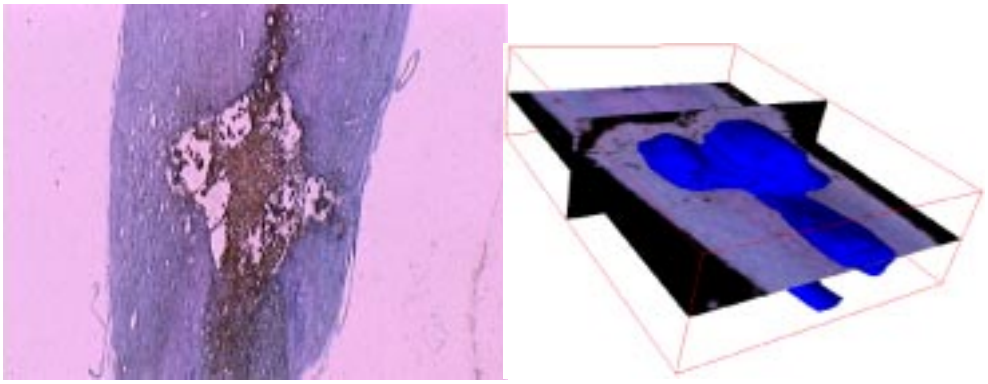

Figure 1.5 (Left) Histological sample of a rat spine. (Right) Reconstruced spinal lesion within slices of 3D histological volume.

Chapter 4 reviews the shape analysis and visualization of free form surface models used in computer aided geometric design and computer graphics. The analysis tools prove essential to detecting surface imperfections aswell as higher order interpatch smoothness. Related research on free-form surfaces visualization are addressed in [BR94, BBB+97].

Three special cases of volumetric quantification which are prevalent in data visualization applications apply to the following data types:

- **Contours** - surfaces which are created through isocontouring of scalar data
- **Slices** - surfaces which are formed by tiling multiple planar cross sections of objects
- **Union of Balls** - also known as the solvent accessible surface and common in molecular visualization

Contour Quantification

Bajaj, Pascucci and Schikore [BPS97] introduce the systematic quantification of metric properties of volumetric data and the relative isocontours. Given an isovalue w one can compute the surface area of the corresponding isosurface, the volume of the *inside region* or any other metric property (also called signature) function of w. The plot of the signatures gives rise to an interface that drives the user in the direct selection of *interesting* isovalues. Figure 1.6 shows the direct selection of noiseless isosurfaces corresponding to skin and bone tissues which correspond to the maxima of the gradient-weighted area signature.

Sliced Data

Objects are frequently reconstructed from serial sections [BCL96b, BCL96a]. In this case, volume properties can be accurately computed using the following equation for

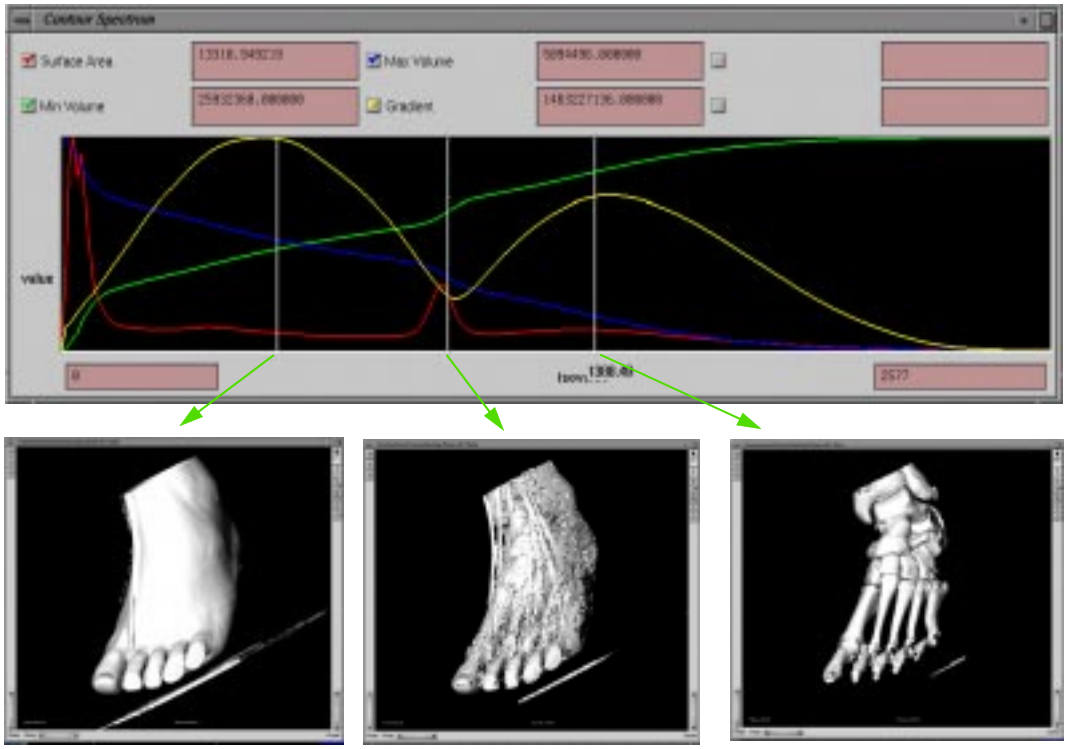

Figure 1.6 Three isosurfaces of the same volumetric MRI scan. The vertical bars in the spectrum interface (top) mark the selected isovalues.

prismatoids, a triangular tiling of two parallel contours: $V = \frac{h}{6}(B_1 + 4M + B_2)$ where B_1 is the area of lower base, B_2 is the area of upper base, M is the area of the midsection joining the bases, and h is the separation between the contours. With n parallel slices of contours equally spaced, the composite volume computation results in: $V' = \frac{h}{6}(B_1 + 4\sum_1^{n-1} M_i + 2\sum_2^{n-1} B_i + B_n)$.

Union of Balls

The geometric, combinatorial and quantitative structure of the union of a set of balls has been presented by [Ede95, DE95]. The union of balls model is equivalent to the space filling model used to represent molecules where each atom is approximated by a ball with a relative van der Waals radius. Deeper insight on the properites of a molecule in solution is provided by the computation of the Solvent Accessible Surface and the Solvent Excluded Surface [SSO96]. The two surfaces are defined by idealizing the solvent molecule (e.g. water) as a single ball and computing the boundary of the region that can be accessed by the solvent center (Solvent Accessible offset of the Union of Balls model of the molecule) or the boundary of the region that cannot be reached by any point of the solvent (Solvent Excluded). On the basis of the union of balls model

exact representation of both the surfaces can be computed efficiently [BLMP97] (see fig. 1.7).

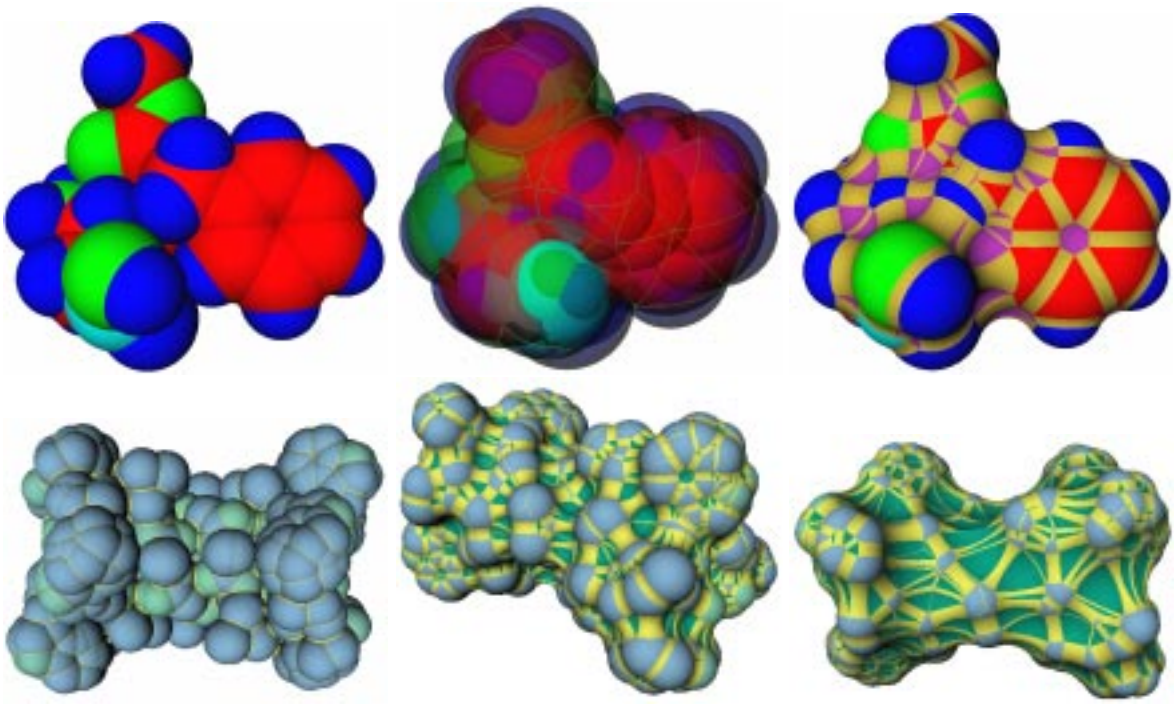

Figure 1.7 (top) Union of Balls, Solvent Accessible and Solvent excluded surfaces of the Nutrasweet molecule with respect to the same solvent. (bottom) Solvent excluded surface of the Gramicidin molecule with respect to three increasing solvent radii.

1.6 Data Reduction

Mesh reduction or simplification refers to a broad category of techniques designed to trade space and complexity for accuracy in representation of a surface or volume mesh. Like isocontouring mesh reduction is an algorithmic approach used to preprocess the input dataset to make more suitable for display or analysis queries. The difference is that while isocontouring extracts an *interesting* feature like a particular isosurface from a volumetric dataset, mesh reduction is meant to generate a reduced version of the volume itself to speedup postprocessing. Figure 1.8 demonstrates mesh reduction applied to 2D functional data, in this case a slice of MRI data. Related results come from several research communities, including Geographical Information Systems (GIS), Computational Fluid Dynamics (CFD), and Virtual Environments/Virtual Reality (VE/VR). Each community has much the same goal for achieving interactivity with very large sets of data. An initial classification of techniques can be made by distinguishing between static simplification, in which a single resolution output is computed from a high-resolution input based on given simplification criteria, and dynamic

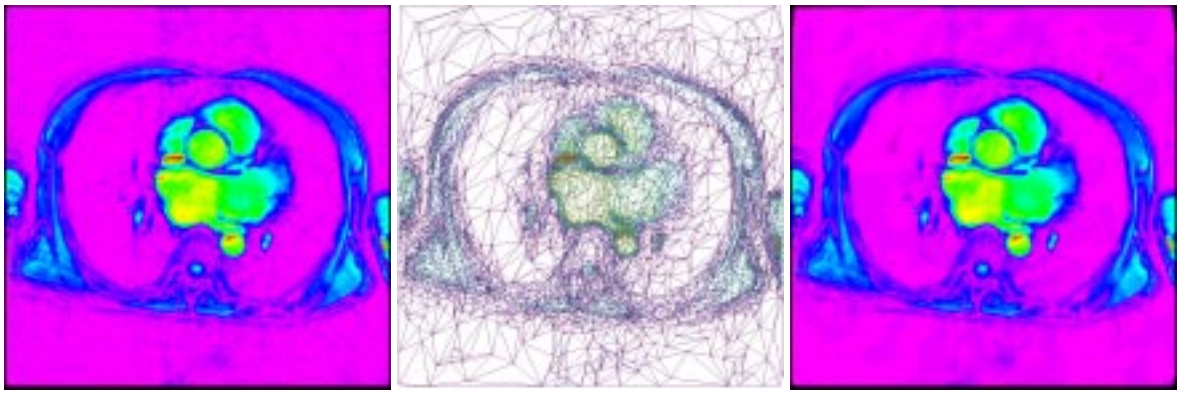

Figure 1.8 Original data (left) Reduced Triangulation (center) Reduced Image (right).

simplification, in which hierarchical triangulations are computed, from which reduced triangulations can be rapidly extracted depending on time dependent metrics such as distance from the viewer, location in the field of view, and approximation error tolerance.

Height-field reduction: A driving application for reduction of height-fields is GIS. A wide range of techniques are based on extraction of key points or edges from the originally dense set of points, followed by a constrained Delaunay triangulation [DFP85, FFNP84, FL79, PDDT94, Tsa93, WJ92]. Silva, et. al [SMK95] uses a greedy method for inserting points into an initially sparse mesh, reporting both better and faster reduction compared to a freely available terrain reduction tool. A survey by Lee [Lee91] reviews methods for computing reduced meshes by both point insertion and point deletion. Bajaj and Schikore [BS95, BS96a] developed practical techniques for measuring the local errors introduced by simplification operations and bound the global error accumulated by multiple applications. Their techniques begin with simple scalar fields and extend easily to multi-valued fields and defined on arbitrary surfaces. Geometric error in the surface as well as functional error in the data are bounded in a uniform manner. Topology preserving, error-bounded mesh simplification have also been explored [BS97]. Figure 1.9 demonstrates geometric mesh reduction while Figure 1.8 demonstrates mesh reduction applied to 2D functional data.

Geometry reduction: Geometric mesh reduction has been approached from several directions. In the reduction of polygonal models, Turk [Tur92] used point repulsion on the surface of a polygonal model to generate a set of vertices for retriangulation. Schroeder, et al. [SZL92] decimate dense polygonal meshes, generated by Marching Cubes [LC87], by deletion of vertices based on an error criteria, followed by local retriangulation with a goal of maintaining good aspect ratio in the resulting triangulation. Errors incurred from local retriangulation are not propagated to the simplified mesh, hence there is no global error control. Rossignac, et al. [RB93] uses clustering and merging of features of an object which are geometrically close, but may not be topologically connected. In this scheme, long thin objects may collapse to an edge and small objects may contract to a point. Hamann [Ham94] applies a similar technique in which triangles are considered for deletion based on curvature estimates at the vertices. Reduction may be driven by mesh resolution or, in the case of functional

Figure 1.9 Three snapshots of geometric mesh simplification of an engine block

surfaces, root-mean-square error. He, et al. [HHK+95] perform mesh reduction by volume sampling and low-pass filtering an object. A multi-resolution triangle mesh is extracted from the resulting multi-resolution volume buffer using traditional isosurfacing techniques. Hoppe, et al. [HDD+93] perform time-intensive mesh optimization based on the definition of an energy function which balances the need for accurate geometry with the desire for compactness in representation. The level of mesh simplification is controlled by parameters in the energy function which penalizes meshes with large numbers of vertices, as well as a spring constant which helps guide the energy minimization to a desirable result.

In [Hop96], Hoppe introduces *Progressive Meshes*, created by applying optimization with the set of basic operations reduced to only an *edge contraction*. Scalar attributes are handled by incorporating them into the energy function. Ronfard, et. al [RR96] also apply successive edge contraction operations to compute a wide range of levels-of-detail for triangulated polyhedra. Edges are extracted from a priority queue based on a computed *edge cost* such that edges of lesser significance are removed first. Cohen, et al. [CVM+96] introduce *Simplification Envelopes* to guide mesh simplification with global error bounds. Envelopes are an extension of *offset surfaces* which serve as an extreme boundary for the desired simplified surface. Lindstrom, et. al [LKR+96] impose a recursive triangulation on a regular terrain and compute preprocessing metrics at various levels of resolution which permits real-time adaptive triangulation for interactive fly-through. Funkhouser et al. describe adaptive display algorithms for rendering complex environments at a sustained frame rate using multiple levels of detail [FS93].

Delaunay techniques for static simplification have been extended to create hierarchies of Delaunay triangulations from which a simplified mesh can be extracted on the fly [dBD95]. Successive levels of the hierarchy are created by deleting points from the current level and retriangulating according to the Delaunay criteria, giving the hierarchical structure of a *directed acyclic graph* (DAG). Puppo improves on the approach of de Berg by augmenting the DAG with information on which triangles between successive resolutions are overlapping [Pup96]. With this information, the problem of extracting a triangulation from the DAG is simplified and requires no backtracking. It is shown that for a given triangulation criteria, the optimal triangulation satisfying the criteria which is embedded in the DAG can be extracted in optimal time. Cohen

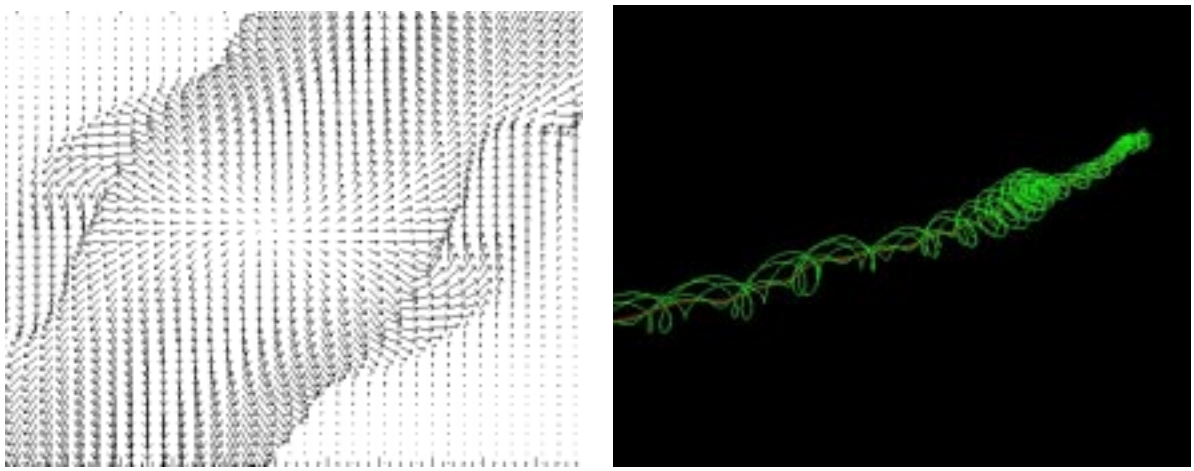

(a) (b)

Figure 1.10 (a) Arrow plot of a two dimensional vector field (b) Streamline along focus in the vortex core surrounded by nearby streamlines.

and Levanoni adopt a tree representation for hierarchical Delaunay triangulation and demonstrate techniques for maintaining temporal coherence between successive triangulations [COL96]. The technique is demonstrated for relatively sparse terrains, and it remains to be seen whether the constraints imposed by a tree representation will restrict simplification for dense triangulated terrains.

Wavelets [Mal89, Dau92] have been utilized for their multiresolution applications in many areas of computer graphics and visualization [SDS96], including image compression [DJL92a], surface description [DJL92b, EDD+95, CPD+96], tiling of contours [Mey94] and curve and surface editing [FS94, ZSS97]. A number of multiresolution volume hierarchies have been proposed for developing adaptive volume rendering and isocontouring [Mur92, Mur95, CDM+94, WV94].

1.7 Topology

Field topology refers to the analysis and classification of critical points and computation of relationships between the critical points of field data [Del94]. Computation and display of field topology can provide a compact global view of what is otherwise a very large set of data. Techniques such as volume rendering and line integral convolution provide qualitative global views of field topology.

Vector Topology: Given a continuous vector field, the locations at which the vector becomes zero are called critical points. Analysis of the critical points can determine behavior of the vector field in the local region. In a 2D vector field, critical points are classified into *sources*, *sinks*, and *saddles* (see Figure 1.11(a)), with both spiral and non-spiral cases for sources and sinks [HH90, HH89, GLL91]. In 3D, additional critical

points include the *spiral-saddle* [HH90], which is useful for locating vortex cores, as shown in Figure 1.10.

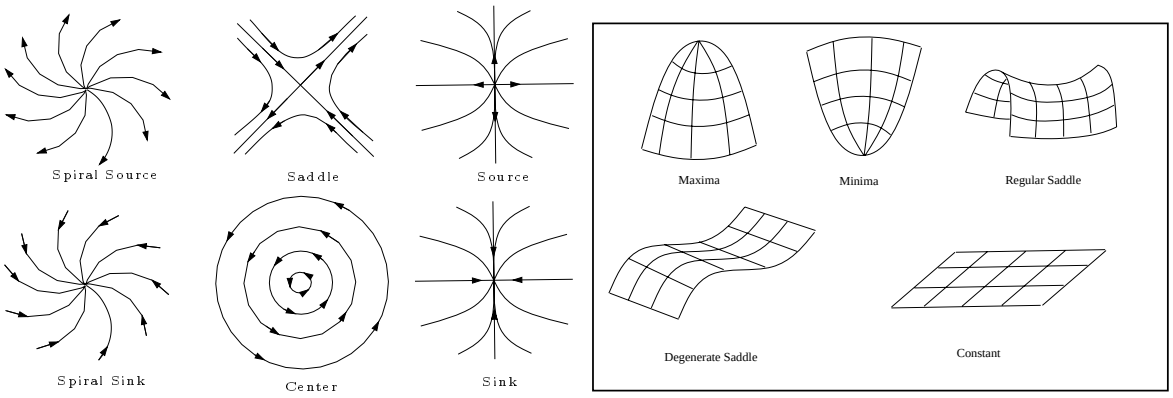

Figure 1.11 (a) Classification of Vector Field zeroes. (b) Critical point classification for Scalar Field.

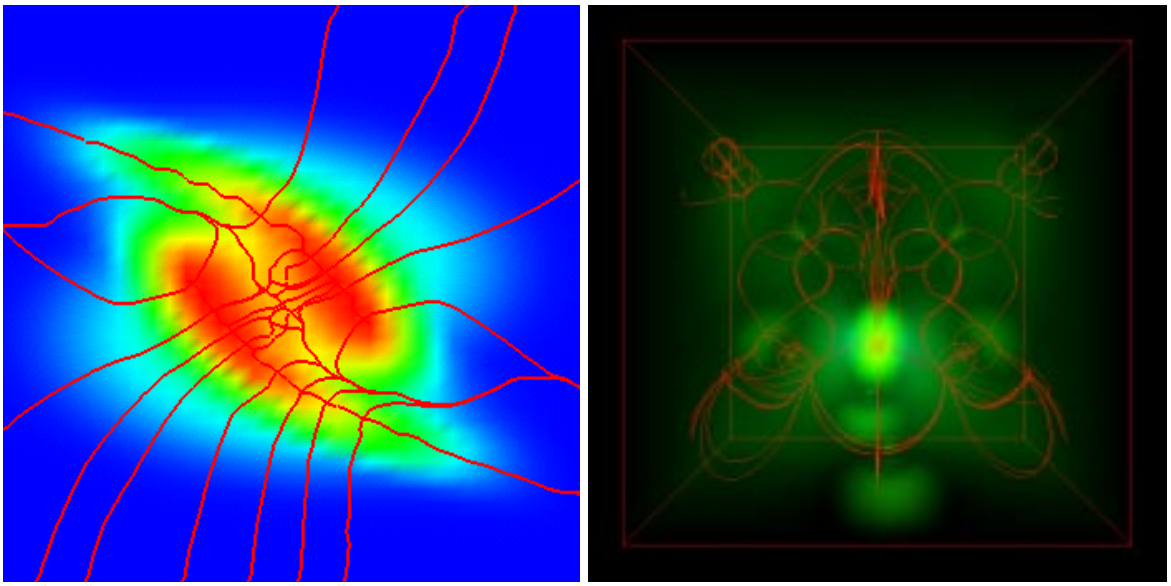

Figure 1.12 Two examples of scalar topology of 2D (left) and 3D (right) scalar fields. The 2D case shows the scalar topology displayed over a color-map of the density in a pion collision simulation. The 3D case is that of the scalar topology diagram of the wave function computed for a high potential iron protein.

Scalar Topology: Scalar field topology can be viewed as a special case of vector field topology, where the vector field is given by the gradient of the scalar function [BS96b]. Critical points in a scalar field are defined by a zero gradient, and can be classified into *maxima*, *minima*, *saddle points*, and degenerate cases, as illustrated in Figure 1.11(b). Two examples are given in Figure 1.12.

1.8 Functions on surfaces

Functions on surface visualization deals with the visual display of scalar functions whose domain is restricted to an arbitrary geometric surface in three dimensions. The surface may be the isosurface of another scalar field, or simply a geometric domain with an associated function field [FLN+90, BOP92, BX94, BBX95].

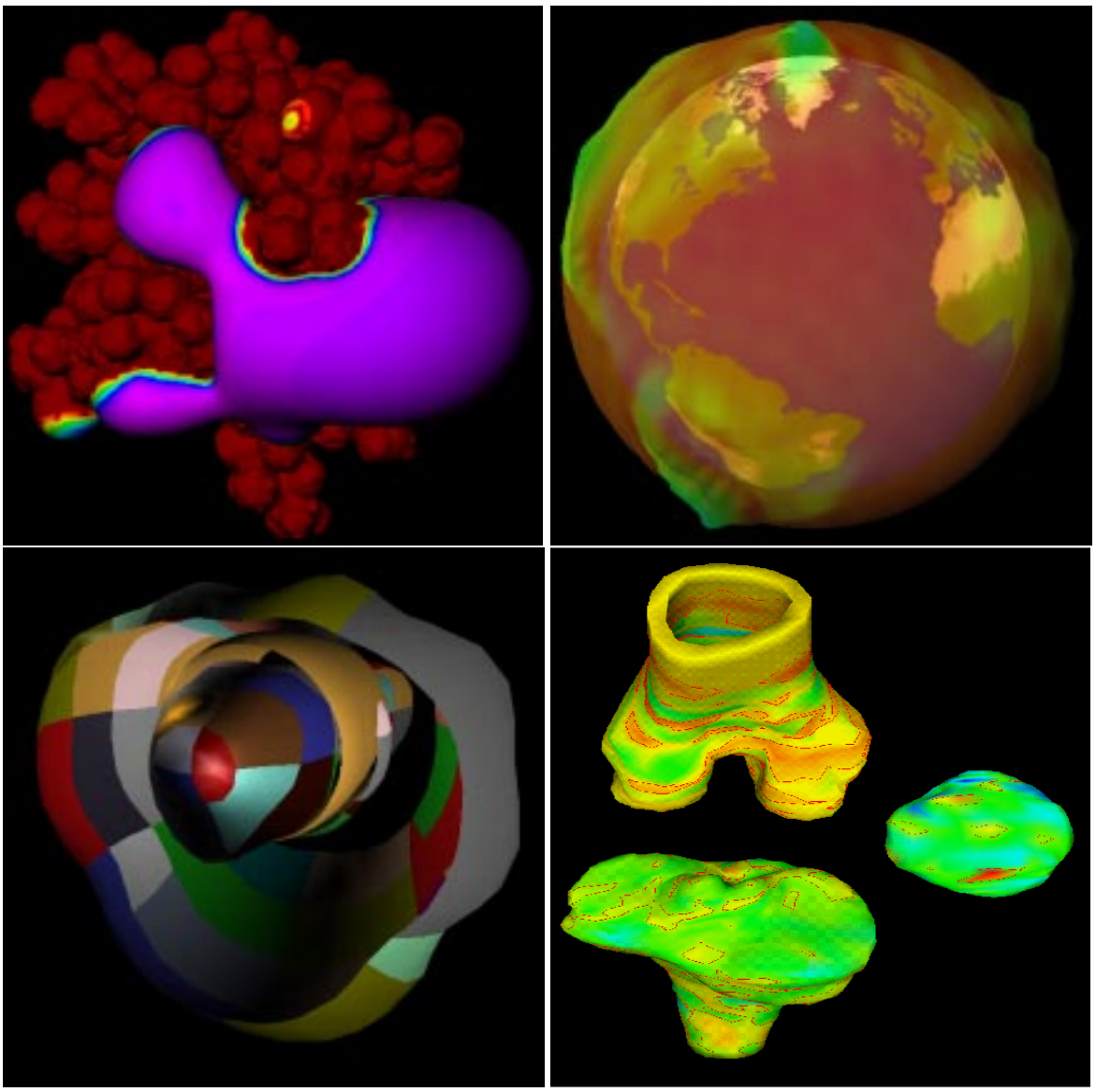

Figure 1.13 Visualiztion of functions on surfacea. (top-left) The electrostatic energy potential shown on an isosurface of van der Waals interaction potenial energy. (top-right) Pressure distribution around the earth globe. (bottom-left) Pressure distribution on the surface of a jet engine modeled and displayed using tensor product surface splines. (bottom-right) Stress distribution on a human knee joint based on static loads.

2

Efficient Techniques for Volume Rendering of Scalar Fields

DATA VISUALIZATION TECHNIQUES, Edited by C. Bajaj

3

Accelerated IsoContouring of Scalar Fields

DATA VISUALIZATION TECHNIQUES, Edited by C. Bajaj

4

Surface Interrogation: Visualization Techniques for Surface Analysis

DATA VISUALIZATION TECHNIQUES, Edited by C. Bajaj

5

Vector Field Visualization Techniques

DATA VISUALIZATION TECHNIQUES, Edited by C. Bajaj

6

Applications of Texture Mapping to Volume and Flow Visualization

DATA VISUALIZATION TECHNIQUES, Edited by C. Bajaj

7

Continuous Bayesian Tissue Classification for Visualization

DATA VISUALIZATION TECHNIQUES, Edited by C. Bajaj

References

[Baj88] C. Bajaj. Geometric modeling with algebraic surfaces. In D. Handscomb, editor, *The Mathematics of Surfaces III*, pages 3–48. Oxford Univ. Press, 1988.

[BBB+97] J. Bloomenthal, C. L. Bajaj, J. Blinn, M.-P. Cani-Gascuel, A. Rockwood, B. Wyvill, and G. Wyvill. *Introduction to Implicit Surfaces*. Morgan Kaufman Publishers, 1997.

[BBX95] C. L. Bajaj, F. Bernardini, and G. Xu. Automatic reconstruction of surfaces and scalar fields from 3D scans. In R. Cook, editor, *SIGGRAPH 95 Conference Proceedings*, Annual Conference Series, pages 109–118. ACM SIGGRAPH, Addison Wesley, August 1995. held in Los Angeles, California, 06-11 August 1995.

[BCL96a] C. L. Bajaj, E. J. Coyle, and K.-N. Lin. Surface and 3D triangular meshes from planar cross sections. In *Proc. of the 5th International Meshing Roundtable*, number SAND96-2301 UC-405 in Sandia Report, pages 169–178, 1996.

[BCL96b] C. L. Bajaj, E. J. Coyle, and K.-N. Lin. Arbitrary topology shape reconstruction from planar cross sections. *Graphical Models and Image Processing*, 6(58):524–543, November 1996.

[BLMP97] C. Bajaj, H. Y. Lee, R. Merkert, and V. Pascucci. NURBS based B-rep models for macromolecules and their properties. In C. Hoffmann and W. Bronsvort, editors, *Proceedings of the 4th Symposium on Solid Modeling and Applications*, pages 217–228, New York, May14–16 1997. ACM Press.

[BOP92] R. Barnhill, K. Opitz, and H. Pottmann. Fat surfaces: a trivariate approach to triangle-based interpolation on surfaces. *Computer Aided Geometric Design*, 9:365–378, 1992.

[Bow95] J. E. Bowie, editor. *Data Visualization in Molecular Science*. Addison-Wesley Publishing Company, 1995.

[BPS97] C. L. Bajaj, V. Pascucci, and D. R. Schikore. The contour spectrum. In *Proceedings of IEEE Visualization '97*, pages 167–173, October 1997.

[BR94] C. Bajaj and A. Royappa. *Triangulation and Display of Arbitrary Rational Parametric Surfaces*. In R. Bergeron, A. Kaufman, editor, Proc. of IEEE Visualization '94 Conference, 1994.

[BS95] C. L. Bajaj and D. R. Schikore. Decimation of 2d scalar data with error control, 1995.

[BS96a] C. L. Bajaj and D. R. Schikore. Error-bounded reduction of triangle meshes with multivariate data. In *Proceedings of SPIE Symposium on Visual Data Exploration and Analysis III*, 1996.

[BS96b] C. L. Bajaj and D. R. Schikore. Visualization of scalar topology for structural enhancement, 1996.

[BS97] ———. Topology preserving data simplification with error bounds, 1997.

[BX94] C. Bajaj and G. Xu. Modeling Scattered Function Data on Curved Surface. In J. Chen, N. Thalmann, Z. Tang, and D. Thalmann, editor, Fundamentals of Computer Graphics, pages 19 – 29, Beijing, China, 1994.

[CDM+94] P. Cignoni, L. De Floriani, C. Montoni, E. Puppo, and R. Scopigno. Multiresolution modeling and visualization of volume data based on simplicial complexes. In A. Kaufman and W. Krueger, editors, *1994 Symposium on Volume Visualization*,

pages 19–26. ACM SIGGRAPH, October 1994. ISBN 0-89791-741-3.

[Cle93] W. S. Cleveland. *Visualizing Data*. Hobart Press, Summit, New Jersey, 1993.

[COL96] D. Cohen-Or and Y. Levanoni. Temporal continuity in levels of detail. In R. Yagel and G. M. Nielson, editors, *Visualization '96 Proceedings*, pages 37–42, 1996.

[CPD+96] A. Certain, J. Popović, T. DeRose, T. Duchamp, D. Salesin, and W. Stuetzle. Interactive multiresolution surface viewing. In H. Rushmeier, editor, *SIGGRAPH 96 Conference Proceedings*, Annual Conference Series, pages 91–98. ACM SIGGRAPH, Addison Wesley, August 1996. held in New Orleans, Louisiana, 04-09 August 1996.

[CVM+96] J. Cohen, A. Varshney, D. Manocha, G. Turk, H. Weber, P. Agarwal, Frederick P. Brooks, Jr., and W. Wright. Simplification envelopes. In H. Rushmeier, editor, *SIGGRAPH '96 Conference Proceedings*, Annual Conference Series, pages 119–128, 1996. held in New Orleans, LA, August 4-9, 1996.

[Dau92] I. Daubechies. *Ten Lectures on Wavelets*, volume 61 of *CBMS-NSF Regional Conference Series in Applied Mathematics*. Society for Industrial and Applied Mathematics, Philadelphia, 1992.

[dBD95] M. de Berg and K. Dobrindt. On levels of detail in terrains. In *Proc. 11th Annu. ACM Sympos. Comput. Geom.*, pages C26–C27, 1995.

[DE95] Delfinado and Edelsbrunner. An incremental algorithm for betti numbers of simplicial complexes on the 3-sphere. *Computer Aided Geometric Design*, 12, 1995.

[Del94] T. Delmarcelle. *The Visualization of Second-Order Tensor Fields*. PhD thesis, Stanford University, 1994. Ginzton Lab Report 5228.

[DFP85] L. DeFloriani, B. Falcidieno, and C. Pienovi. Delaunay-based representation of surfaces defined over arbitrarily shaped domains. *Computer Vision, Graphics and Image Processing*, 32:127–140, 1985.

[DJL92a] R. DeVore, B. Jawerth, and B. J. Lucier. Image compression through wavelet transform coding. *IEEE Transactions on Information Theory*, 38:719–746, 1992.

[DJL92b] R. A. DeVore, B. Jawerth, and B. J. Lucier. Surface compression. *Computer Aided Geometric Design*, 9:219–239, 1992.

[EDD+95] M. Eck, T. DeRose, T. Duchamp, H. Hoppe, M. Lounsbery, and W. Stuetzle. Multiresolution analysis of arbitrary meshes. In R. Cook, editor, *SIGGRAPH 95 Conference Proceedings*, Annual Conference Series, pages 173–182. ACM SIGGRAPH, Addison Wesley, August 1995. held in Los Angeles, California, 06-11 August 1995.

[Ede95] Edelsbrunner. The union of balls and its dual shape. *GEOMETRY: Discrete & Computational Geometry*, 13, 1995.

[FFNP84] L. D. Floriani, B. Falcidieno, G. Nagy, and C. Pienovi. A hierarchical structure for surface approximation. *Computers and Graphics*, 8(2):183–193, 1984.

[FL79] R. J. Fowler and J. J. Little. Automatic extraction of irregular network digital terrain models. In *Computer Graphics (SIGGRAPH '79 Proceedings)*, volume 13(3), pages 199–207, 1979.

[FLN+90] T. Foley, D. Lane, G. Nielson, R. Franke, and H. Hagen. Interpolation of scattered data on closed surfaces. *Computer Aided Geometric Design*, 7:303–312, 1990.

[FS93] T. A. Funkhouser and C. H. Sequin. Adaptive display algorithm for interactive frame rates during visualization of complex virtual environments. In *Computer Graphics (SIGGRAPH '93 Proceedings)*, volume 27, pages 247–254, 1993.

[FS94] A. Finkelstein and D. H. Salesin. Multiresolution curves. In A. Glassner, editor, *Proceedings of SIGGRAPH '94 (Orlando, Florida, July 24–29, 1994)*, Computer Graphics Proceedings, Annual Conference Series, pages 261–268. ACM SIGGRAPH, ACM Press, July 1994. ISBN 0-89791-667-0.

[GLL91] A. Globus, C. Levit, and T. Lasinski. A tool for visualizing the topology of three-dimensional vector fields. In G. M. Nielson and L. Rosenblum, editors, *Visualization '91 Proceedings*, pages 33–40, 1991.

[Ham94] B. Hamann. A data reduction scheme for triangulated surfaces. In *Computer Aided Geometric Design*, volume 13, pages 197–214. 1994.

[HDD+93] H. Hoppe, T. DeRose, T. Duchamp, J. McDonald, and W. Stuetzle. Mesh optimization. In J. T. Kajiya, editor, *Computer Graphics (SIGGRAPH '93 Proceedings)*, volume 27, pages 19–26, 1993.

[HH89] J. Helman and L. Hesselink. Representation and display of vector field topology in fluid flow data sets. *IEEE Computer*, 12(8):27–36, 1989.

[HH90] J. L. Helman and L. Hesselink. Surface representations of two- and three-dimensional fluid flow topology. In *Proceedings of Visualization '90*, pages 6–13, 1990.

[HHK+95] T. He, L. Hong, A. E. Kaufman, A. Varshney, and S. Wang. Voxel based object simplification. In G. M. Nielson and D. Silver, editors, *Visualization '95 Proceedings*, pages 296–303, 1995.

[Hop96] H. Hoppe. Progressive meshes. In H. Rushmeier, editor, *SIGGRAPH '96 Conference Proceedings*, Annual Conference Series, pages 99–108, 1996. held in New Orleans, Louisiana, August 4-9, 1996.

[HU94] H. M. Hearnshaw and D. J. Unwin, editors. *Visualization in Graphical Information Systems*. John Wiley & Sons, 1994.

[KK93] P. R. Keller and M. M. Keller. *Visual Cues: Practical Data Visualization*. IEEE Computer Society Press and IEEE Press, 1993.

[KM92] D. Kenwright and G. Mallinson. A 3-D streamline tracking algorithm using dual stream functions. In A. E. Kaufman and G. Nielson, editors, *Proceedings of IEEE Visualization '92 (Boston, Massachusetts, October 19–23, 1992)*, Visualization Conference Series, pages 62–68, 1992.

[LC87] W. E. Lorensen and H. E. Cline. Marching cubes: A high resolution 3D surface construction algorithm. In M. C. Stone, editor, *Computer Graphics (SIGGRAPH '87 Proceedings)*, volume 21, pages 163–169, 1987.

[Lee91] J. Lee. Comparison of existing methods for building triangular irregular networks. *Int. Journal of Geographical Information Systems*, 5(2):267–285, 1991.

[Lev92] M. Levoy. Volume rendering using the Fourier projection-slice theorem. In *Proceedings of Graphics Interface '92*, pages 61–69, 1992.

[LKR+96] P. Lindstrom, D. Koller, W. Ribarsky, L. F. Hodges, N. Faust, and G. A. Turner. Real-time, continuous level of detail rendering of height fields. In H. Rushmeier, editor, *SIGGRAPH '96 Conference Proceedings*, Annual Conference Series, pages 109–118, 1996. Held in New Orleans, Louisiana, August 4-9, 1996.

[Mal89] S. G. Mallat. A theory for multiresolution signal decomposition: The wavelet representation. *IEEE Transactions on Pattern Analysis and Machine Intelligence*, 11(7):674–693, July 1989.

[Mal93] T. Malzbender. Fourier volume rendering. *ACM Transactions on Graphics*, 12(3):233–250, 1993.

[Mey94] D. Meyers. Multiresolution tiling. In *Proceedings of Graphics Interface '94*, pages 25–32, Banff, Alberta, Canada, 1994.

[Mur92] S. Muraki. Approximation and rendering of volume data using wavelet transforms. In A. E. Kaufman and G. M. Nielson, editors, *Proceedings of Visualization '92 (Boston, Massachusetts, October 19–23, 1992)*, pages 21–28. IEEE Computer Society, IEEE Computer Society Press, October 1992.

[Mur95] S. Muraki. Multiscale volume representation by a DoG wavelet. *IEEE Transactions on Visualization and Computer Graphics*, 1(2):109–116, June 1995. ISSN 1077-2626.

[NHM97] G. M. Nielson, H. Hagen, and H. Muller, editors. *Scientific Visualization*. IEEE Computer Society, 1997.

[PDDT94] E. Puppo, L. Davis, D. DeMenthon, and Y. Teng. Parallel terrain triangulation. *Int. Journal of Geographical Information Systems*, 8(2):105–128, 1994.

[Pup96] E. Puppo. Variable resolution terrain surfaces. In F. Fiala, E. Kranakis, and J.-R. Sack, editors, *Canadian Conference on Computational Geometry*, pages 202–210, 1996.

[RB93] J. Rossignac and P. Borrel. Multi-resolution 3D approximations for rendering complex scenes. In *IFIP TC 5.WG 5.10 II Conference on Geometric Modeling*

in Computer Graphics, 1993. IBM Research Report RC 17697, Yorktown Heights, NY 10598.

[REE+94] L. Rosenblum, R. A. Earnshaw, J. Encarnacao, H. Hagen, A. Kaufman, S. Klimenko, G. Nielson, F. Post, and D. Thalmann, editors. *Scientific Visualization : Advances and Challenges*. Academic Press, 1994.

[RR96] R. Ronfard and J. Rossignac. Full-range approximation of triangulated polyhedra. In *Eurographics '96*, volume 15. 1996.

[SDS96] E. J. Stollnitz, T. D. DeRose, and D. H. Salesin. Wavelets for computer graphics: Theory and applications, 1996.

[SMK95] C. Silva, J. Mitchell, and A. E. Kaufman. Automatic generation of triangular irregular networks using greedy cuts. In G. M. Nielson and D. Silver, editors, *Visualization '95 Proceedings*, pages 201–208, 1995.

[SSO96] M. Sanner, J.-C. Spehner, and A. Olson. Reduced surface: an efficient way to compute molecular surfaces. *Biopolymers*, 38(3):305–320, 1996.

[SZL92] W. J. Schroeder, J. A. Zarge, and W. E. Lorensen. Decimation of triangle meshes. In E. E. Catmull, editor, *Computer Graphics (SIGGRAPH '92 Proceedings)*, volume 26(2), pages 65–70, 1992.

[TL93] T. Totsuka and M. Levoy. Frequency domain volume rendering. In J. T. Kajiya, editor, *Computer Graphics (SIGGRAPH '93 Proceedings)*, volume 27, pages 271–278, August 1993.

[Tsa93] V. J. D. Tsai. Delaunay triangulations in TIN creation: an overview and a linear-time algorithm. *Int. Journal of Geographical Information Systems*, 7(6):501–524, 1993.

[Tur92] G. Turk. Re-tiling polygonal surfaces. In E. E. Catmull, editor, *Computer Graphics (SIGGRAPH '92 Proceedings)*, volume 26(2), pages 55–64, 1992.

[Wat92] D. F. Watson. *Contouring*. Pergamon, 1992.

[WJ92] J. M. Ware and C. B. Jones. A multiresolution topographic surface database. *Int. Journal of Geographical Information Systems*, 6(6):479–496, 1992.

[WV94] J. Wilhelms and A. Van Gelder. Multi-dimensional trees for controlled volume rendering and compression. In A. Kaufman and W. Krueger, editors, *1994 Symposium on Volume Visualization*, pages 27–34. ACM SIGGRAPH, October 1994. ISBN 0-89791-741-3.

[ZSS97] D. Zorin, P. Schröder, and W. Sweldens. Interactive multiresolution mesh editing. In T. Whitted, editor, *SIGGRAPH 97 Conference Proceedings*, Annual Conference Series, pages 259–268. ACM SIGGRAPH, Addison Wesley, August 1997. ISBN 0-89791-896-7.